

# Synthesis, characterization and catalytic property of manganese dioxide with different structures

Youcun Chen · Zhongyu Duan · Yulin Min ·  
Mingwang Shao · Yingguo Zhao

Received: 7 September 2010 / Accepted: 14 December 2010 / Published online: 7 January 2011  
© Springer Science+Business Media, LLC 2011

**Abstract** In this paper, different crystallographic types and crystal morphologies of MnO<sub>2</sub> nanomaterials have been selectively synthesized by a simple hydrothermal route.  $\alpha$ -MnO<sub>2</sub> nanowires, and  $\gamma$ -MnO<sub>2</sub> hollow hierarchical spheres have been prepared by a sodium dodecyl benzenesulfonate (SDBS)-assisted hydrothermal treatment method. The as-synthesized samples were characterized by XRD, SEM, TEM, and HRTEM. Furthermore, the obtained different kinds of MnO<sub>2</sub> nanostructures were found to exhibit favorable photocatalytic activity in organic dyestuff such as methyl orange, showing potential applications in photocatalysis. And the results showed that  $\gamma$ -MnO<sub>2</sub> hollow micro-spheres exhibited superior photocatalytic activities to  $\alpha$ -MnO<sub>2</sub>.

## 1 Introduction

Nanostructures have aroused great attention not only for their fundamental scientific significance but also for the many technological applications that derive from their fascinating properties, superior to the corresponding bulk counterparts [1, 2]. One-dimensional (1-D) nanostructured and constructing hierarchical structures materials have been intensively investigated as building components in fabricating the next generation of microelectronic and optoelectronic devices because they can be employed as both building units and interconnections [3–10]. 1D nanostructures formed by self-assembled are desirable not only in fundamental research but also in future nanodevice design and fabrication. Because of easily controllable reaction condition and the relatively abundant reactant sources, hydrothermal route might provide many options for large-scale production of nanomaterials with special morphology. And large quantities of inorganic materials including metals, chalcogenides, and metal oxides/hydroxides are obtained in nanoscaled forms through this route [11–13].

In particular, manganese oxides have attracted much attention for their physical and chemical properties and wide applications in catalysis, ion exchange, molecular adsorption, biosensor, and energy storage in secondary batteries [14–21]. It is well-known that manganese dioxide can exist in different structural formations, such as  $\alpha$ -,  $\beta$ -,  $\delta$ -, and  $\gamma$ -types, when the basic structure unit (namely, the [MnO<sub>6</sub>] octahedron) is linked in different ways. Therefore, much effort has been directed toward the preparation of low dimensional MnO<sub>2</sub> nanostructures with different morphologies, such as rods, wires, tubes [22–27].

Although there were numerous reports on the catalytic activities of different MnO<sub>2</sub> crystal structure [28–32], yet

---

**Electronic supplementary material** The online version of this article (doi:[10.1007/s10854-010-0278-5](https://doi.org/10.1007/s10854-010-0278-5)) contains supplementary material, which is available to authorized users.

Y. Chen (✉) · Z. Duan · Y. Min · Y. Zhao  
Anhui Key Laboratory of Functional Coordination Compounds,  
Anqing Normal College, Anqing 246011,  
People's Republic of China  
e-mail: chenyc@aqtc.edu.cn

Y. Chen · Z. Duan · Y. Min · Y. Zhao  
School of Chemistry and Chemical Engineering, Anqing Normal  
College, Anqing 246011, People's Republic of China

M. Shao (✉)  
Institute of Functional Nano & Soft Materials (FUNSOM) and  
Jiangsu Key Laboratory for Carbon-Based Functional Materials  
& Devices, Soochow University, Suzhou, Jiangsu 215123,  
People's Republic of China  
e-mail: mwshao@suda.edu.cn

no unanimous conclusion was reached even now. In this paper, we report a simple hydrothermal method to synthesize different manganese dioxide nanostructure under different conditions, and employed them as photocatalysts in the degradation of methyl orange.

## 2 Experimental section

All chemicals were of analytical grade and were directly used without any treatment. The commercial  $\text{MnO}_2$  powder was purchased from Shanghai Reagent Company. A series of parallel experiments were carried out by altering the reaction parameters such as heating temperature, reactant concentration, and reaction time. In brief, the synthesis process could be described as follows:  $\text{MnSO}_4 \cdot \text{H}_2\text{O}$  (1.5 mmol), and  $\text{KMnO}_4$  (1 mmol) were mixed with 15 mL deionized water, followed by an addition of sodium dodecyl benzenesulfonate (SDBS) (0.05 g) to form a deep-red opaque solution immediately, which were vigorously stirred and then transferred to a 23 mL Teflon-lined autoclave. The autoclave were sealed and heated in an oven at 160–180 °C for 2–12 h and then were allowed to cool to room temperature. The resulting products were collected, washed repeatedly with distilled water and absolute ethanol to remove the possible residues, centrifuged, and dried under vacuum at 60 °C for 4 h. We can obtain the product at 160–180 °C for 6–12 h. And the optimal reaction conditions for the growth of the nanowires were at 160 °C for 6 h.

In another experiment, the precursor of manganese was changed into  $\text{MnCl}_2 \cdot 4\text{H}_2\text{O}$  so that the influence of the product morphology and polymorphic formations could be investigated. The synthesis of  $\gamma\text{-MnO}_2$  was carried out on the basis of the previous work of Li's group [22, 23]. In a typical synthesis of  $\gamma\text{-MnO}_2$ , 0.6 g of  $\text{MnCl}_2 \cdot 4\text{H}_2\text{O}$  and 0.3 g of  $\text{KMnO}_4$  were mixed with 15 mL of distilled water and stirred to form a homogeneous mixture after adding the surfactants, which were then transferred into a 23 mL Teflon-lined stainless steel autoclave and heated at 160 °C for 6 h. The products were collected, washed, and dried and to obtain the  $\gamma\text{-MnO}_2$  of hollow micro-spheres. In addition, according to the above procedure, some experiments were made in the absence of SDBS, no any hollow nanostructure was obtained.

The powder X-ray diffraction (XRD) pattern was measured on a Rigaku D/max 2500 X-ray diffractometer ( $\text{Cu K}\alpha$  radiation,  $\lambda = 0.154178$  nm). Field-emission SEM (FE-SEM) images were taken using JEOL JSM-6700F microscopes operated at the accelerating voltages of 10 kV. Transmission electron microscope (TEM) performed on a Hitachi model H-800 transmission electron microscope (TEM) at an accelerating voltage of 200 kV,

and high-resolution transmission electron microscope (HRTEM) (JEOL-2011) operated at an acceleration voltage of 200 kV. For the sake of convenience, all FE-SEM images are briefly called SEM images later.

## 3 Results and discussion

### 3.1 Composition of the product

The crystal phase of the samples was analyzed by powder X-ray diffraction. Figure 1 shows the XRD patterns of two representative products. All the diffraction peaks in Fig. 1a can be indexed to tetragonal symmetry. The lattice constants and deviation are calculated using the values of 2 theta and diffraction planes via minimizing the sum of squares of residuals in 2 theta. to be  $a = 0.9784 \pm 0.0014$  nm and  $c = 0.2846 \pm 0.0008$  nm, which are in good agreement with the reported data for the pure phase of  $\alpha\text{-MnO}_2$  (JCPDS No.44-0140,  $a = 0.9782$  nm and  $c = 0.2853$  nm). From this pattern, it can be seen that the obtained  $\alpha\text{-MnO}_2$  products are of high purity and good crystallinity.

The XRD pattern in Fig. 1b confirms the formation of  $\gamma\text{-MnO}_2$ . The lattice constants are calculated to be  $a = 0.6367 \pm 0.0013$  nm,  $b = 1.0134 \pm 0.003$  nm,  $c = 0.4099 \pm 0.0019$  nm, which are in good agreement with the reported data for the pure phase of  $\gamma\text{-MnO}_2$  (JCPDS No. 14-0644,  $a = 0.636$  nm,  $b = 1.015$  nm, and  $c = 0.409$  nm). Meanwhile, the peaks of curve b are shown broader, implying smaller crystalloid. The result shows the crystalloid of  $\gamma\text{-MnO}_2$  is not as good as that of  $\alpha\text{-MnO}_2$ . The XRD analysis results are similar to that reported in the literature [22–25].

The chemical reaction involved in our present hydrothermal synthesis may be briefly described as:

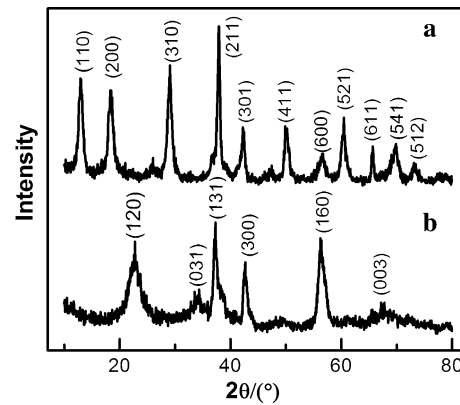
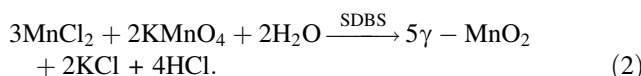
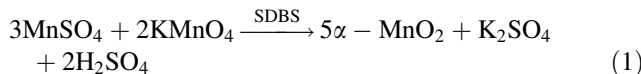


**Fig. 1** XRD patterns of the as-synthesized **a**  $\alpha$ -, and **b**  $\gamma\text{-MnO}_2$  nanostructures



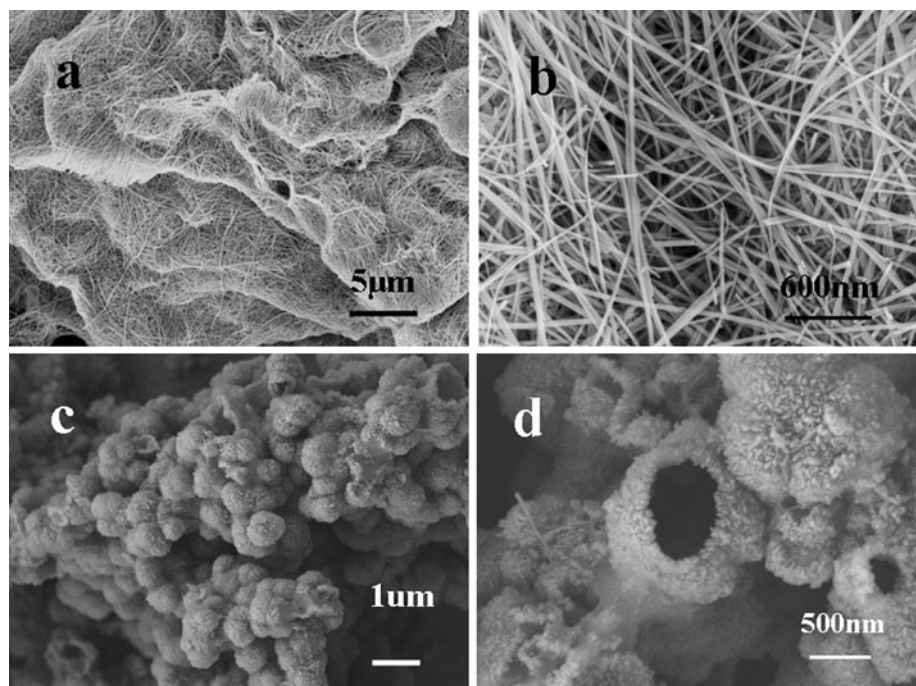
As can be seen in the above equations, the related reactions are quite simple:  $\text{MnO}_2$  have been synthesized by reactions of  $\text{KMnO}_4$  with the assistance of SDBS with different Mn source. The coexisting ions might play an important role in determining the crystal structure of  $\text{MnO}_2$ . There are various examples in the solution synthesis: In Li et al.'s work,  $\text{MnSO}_4$  reacted with  $(\text{NH}_4)_2\text{S}_2\text{O}_8$  to obtained  $\beta\text{-MnO}_2$  in the hydrothermal reaction at  $120^\circ$  for 12 h, while  $\alpha\text{-MnO}_2$  was prepared by adding ammonium sulfate to their reaction system [33]. In the synthesis of CdS nonmaterial, cadmium chloride as starting material may tend to produce  $\alpha\text{-CdS}$  [34], while cadmium sulfate to  $\beta\text{-CdS}$  [35].

As a result, we have obtained large-scale production of  $\text{MnO}_2$  nanostructure with different morphologies for practical application by changing precursor (Fig. 2). Hence, we can easily control the reaction system to synthesize manganese dioxide with desired crystals.

### 3.2 Morphology characterization

The morphologies of the  $\text{MnO}_2$  powders obtained were examined by SEM, TEM, and HRTEM microscopy.

**Fig. 2** **a** and **b** SEM image of the obtained 1-dimensional  $\alpha\text{-MnO}_2$ ; and **c** and **d** SEM image of the obtained 0-dimensional  $\gamma\text{-MnO}_2$



### 3.3 $\alpha\text{-MnO}_2$

Figure 3 shows the SEM images of the as-synthesized 1-D  $\alpha\text{-MnO}_2$  nano- and micromaterials which were synthesized using  $\text{MnSO}_4$  and  $\text{KMnO}_4$  as reactants at  $160^\circ\text{C}$  for 6 h. The SEM images of the as-prepared  $\text{MnO}_2$  clearly reveal the presence of a large quantity of nanowires.  $\alpha\text{-MnO}_2$  single-crystal nanowires with diameters 40–50 nm and lengths ranging between hundreds of nanometres and several micrometers (Fig. 3b, c). Due to the influence of SDBS, Some of nanowires align well to present a form of coaxial nanorops or coiled together (Fig. 3b).

### 3.4 $\gamma\text{-MnO}_2$

The hollow urchins of  $\gamma\text{-MnO}_2$  were fabricated on a large scale when manganese sulfate was changed into manganese chloride (Fig. 4). Hollow interiors can be created via Kirkendall effect [36] after a reaction time of about 6 h, and the ripening process was confirmed by tracking the crystallization and morphology of the product at different reaction stages. In order to investigate the formation mechanism of  $\text{MnO}_2$  hollow micro-spheres, some comparative experiments were carried out at 1 and 6 h keeping the otherwise experimental conditions unchanged. The results show that the product synthesized at  $160^\circ\text{C}$  for 6 h, could be indexed to  $\gamma\text{-MnO}_2$  (Fig. 1b). And the product obtained from 1 h was only nanoparticles.

Under hydrothermal condition,  $\alpha\text{-MnO}_2$  nanowires were obtained via adding surfactant. These nanowires

**Fig. 3** SEM images at different magnifications of  $\alpha\text{-MnO}_2$  nanowires synthesized using  $\text{MnSO}_4\cdot\text{H}_2\text{O}$  as manganese precursor at 160 °C for 6 h

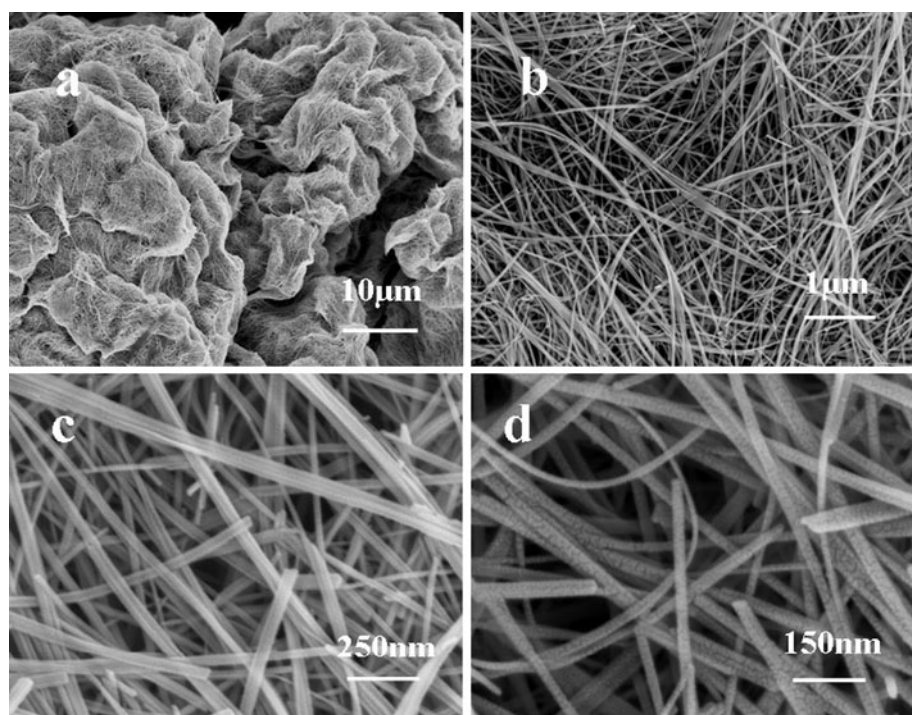
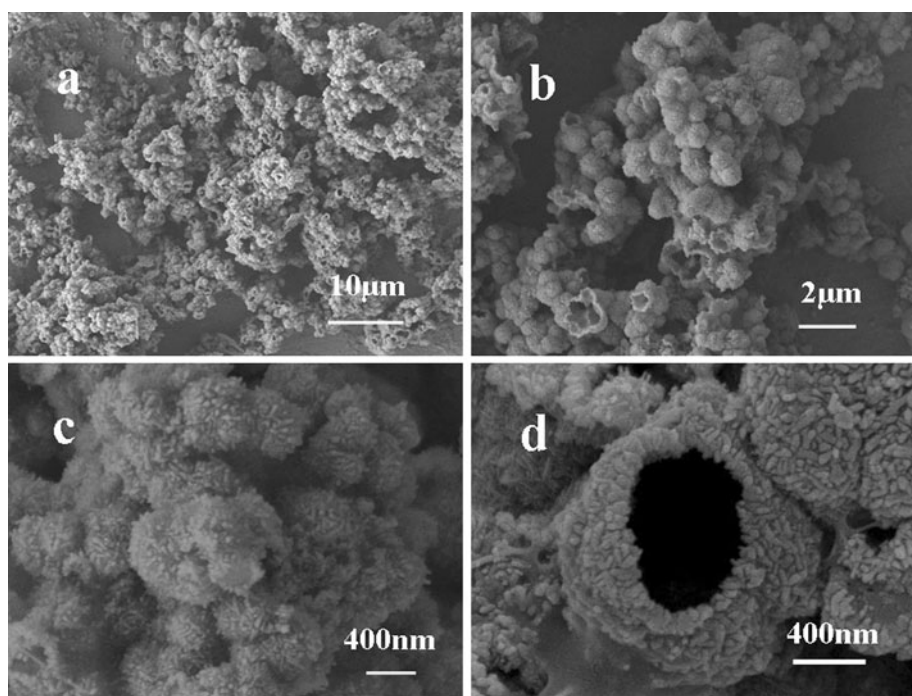


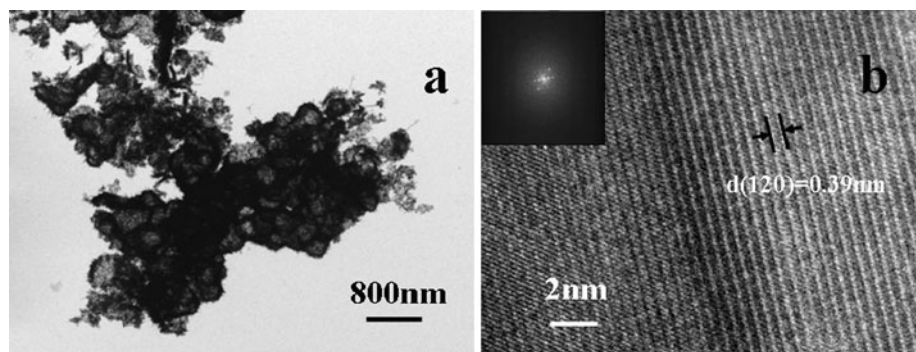
**Fig. 4** **a** Panoramic SEM image, **b** and **c** magnified SEM image; and **d** typical open hollow urchin of the product obtained at 160 °C for 6 h



were longer and coalescent in this experiment. But the hollow urchins of  $\gamma\text{-MnO}_2$  were synthesized using  $\text{MnCl}_2\cdot 4\text{H}_2\text{O}$  without  $\text{SO}_4^{2-}$  existence. In this experiment, the surfactant SDBS is the reason of the formation of this hollow urchin shapes. In addition, some experiments were made in the absence of SDBS. There were nanowires and nanorods presence, but no any hollow nanostructure was obtained.

The morphologies of the products were observed by SEM. Interesting morphologies and microstructures of  $\gamma\text{-MnO}_2$  prepared by hydrothermal reaction for 6 h are observed as shown in Fig. 4. The panoramic morphology of  $\gamma\text{-MnO}_2$  is shown in Fig. 4a, which reveals that the sample has a spherical morphology about 1  $\mu\text{m}$  in diameter (Fig. 4d). The high-magnification images (Fig. 4c) reveal that the surface of the urchin-like sphere consists of

**Fig. 5** **a** TEM images of the hollow urchin of  $\gamma$ -MnO<sub>2</sub>; and **b** HRTEM image from the hollow urchin



numerous compactly growing nanorods, which indicates that the nano-particles could gradually change into nanorods after hydrothermal reaction for 6 h. From the SEM pictures (Fig. 4d), a few spheres with an interior cavity are also observed, suggesting that the as-synthesized  $\gamma$ -MnO<sub>2</sub> spheres might show the hollow structure. As can be seen from its overview, the samples consist predominantly of hollow urchins with visible cavities (Fig. 4b). Hollow urchins consist of the nanorods with the length of 40–100 nm.

The interesting morphology and microstructures of  $\gamma$ -MnO<sub>2</sub> were further studied using TEM. The TEM images of Fig. 5a further confirmed that the  $\gamma$ -MnO<sub>2</sub> was hollow structure. Figure 5b displays the HRTEM image of the hollow urchin of  $\gamma$ -MnO<sub>2</sub>. The lattice spacing of 0.39 nm between adjacent lattice planes corresponds to the distance between two (120) crystal planes. It shows clear lattice fringes, which confirm the single-crystal of the  $\gamma$ -MnO<sub>2</sub>. In addition, the crystallites located in the inner cores, compared to those in the outer surfaces, have high surface energies and thus are easily dissolved. The inner cores provided a MnO<sub>2</sub> source for the durative growth of the nanorods outside, and then the nanorods grew at the expense of the cores inside the spheres. As a result of this process, the size of the crystal cores was reduced gradually while the hollow volume was enlarged. Finally, the hollow urchins were formed with complete depletion of the cores. The Kirkendall effect was observed for those with a longer reaction time (3–6 h), and the inner space of the spheres was further increased.

### 3.5 Catalytic properties

High surface area seems to be an important factor in determining the photocatalytic activity [37, 38]. Considering that the products which have high surface area may contribute to photocatalytic activity, we used the 1-dimensional  $\alpha$ -MnO<sub>2</sub> nanowires and 0-dimensional  $\gamma$ -MnO<sub>2</sub> hollow micro-spheres as photocatalysts, and then examined their photocatalytic activity by measuring the photodegradation of methyl orange solution.

A suspension composed of nanostructured MnO<sub>2</sub> hollow microspheres and 100 mL of methyl orange (10 mg/L) were placed in a 100 mL beaker and irradiated with UV light under continuous stirring. At 20 min intervals, analytical samples were drawn from the beaker and the methyl orange concentration was analyzed using a UV-vis spectrophotometer at a wavelength of 465 nm. Figure 6 shows the degradation rate of methyl orange over nanostructured  $\gamma$ -MnO<sub>2</sub> hollow micro-spheres,  $\alpha$ -MnO<sub>2</sub> nanowires or commercial MnO<sub>2</sub>, which was the results of five experiments. The mass of catalysts was 0.2 g for those three MnO<sub>2</sub> materials. It is obvious that  $\gamma$ -MnO<sub>2</sub> hollow microspheres exhibited superior photocatalytic activities, indicating that the hollow structures assembled by nanorods are favorable for the enhancement of the photocatalytic performance. Figure 6b shows the degradation rate of methyl orange for  $\alpha$ -MnO<sub>2</sub> nanowires. It is not as good as that of  $\gamma$ -MnO<sub>2</sub>, but it is superior to commercial MnO<sub>2</sub> (Fig. 6c).

The slopes of curves a, b and c were calculated as 0.00462, 0.00281 and 0.00125, which shows the degradation rate ratio of  $\gamma$ -MnO<sub>2</sub> hollow micro-spheres :  $\alpha$ -MnO<sub>2</sub> nanowires: commercial MnO<sub>2</sub> is 3.7:2.3:1.

The  $\gamma$ -MnO<sub>2</sub> and  $\alpha$ -MnO<sub>2</sub> show good photocatalytic activity. And the catalytic activity was also affected by the

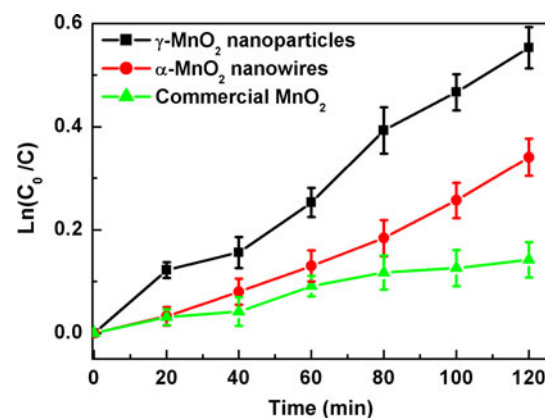


**Fig. 6** The degradation rate of methyl orange over different photocatalysts: **a**  $\gamma$ -MnO<sub>2</sub> hollow micro-spheres, **b**  $\alpha$ -MnO<sub>2</sub> nanowires, and **c** commercial MnO<sub>2</sub>

surface state of the catalyst because the reacting agent was absorbed on the surface of the catalyst before the catalytic reaction. The commercial powder is  $\beta$ -MnO<sub>2</sub> with size of 200–300 nm, as confirmed by XRD pattern (Fig. S1) and SEM image (Fig. S2), respectively. The largest size may be the reason of its worst photocatalysis.

#### 4 Conclusions

In conclusion, the  $\alpha$ -MnO<sub>2</sub> single-crystal nanowires and  $\gamma$ -MnO<sub>2</sub> hollow micro-spheres were directly synthesized by surfactant-assisted method. MnO<sub>2</sub> crystal forms can be synthesized by selected-control reaction conditions, and their crystal phases were confirmed by XRD and TEM measurement. This simple synthetic method can be easily adjusted to synthesize  $\alpha$ -MnO<sub>2</sub> nanowires  $\gamma$ -MnO<sub>2</sub> hollow spheres with different crystal forms on a large scale. We believe that this hydrothermal synthesis of surfactant-assisted method has potential applications for the preparation of other metal oxides with nanostructure and microstructure.

**Acknowledgments** The present work was supported by the special funding support from the National Science Foundation of China (NSFC) (Grants No. 20771006) and Natural Science Foundation of Anhui Province (No. 2006kj042A).

#### References

1. X.Y. Wang, Z.Q. Wang, H.M. Tian, J.Y. Zhang, T. Yu, Z.T. Yu, Z.G. Zou, Chinese J. Inorg. Chem. **25**, 1893 (2009)
2. E.V. Shevchenko, D.V. Talapin, N.A. Kotov, S. O'Brien, C.B. Murray, Nature **439**, 55 (2006)
3. J.T. Hu, T.W. Odom, C.M. Lieber, Acc. Chem. Res. **32**, 435 (1999)
4. P.M. Forster, A.K. Cheetham, Angew. Chem. Int. Ed. **41**, 457 (2002)
5. J.S. Moore, M.L. Kraft, Science **320**, 620 (2008)
6. X. Wang, J. Zhuang, Q. Peng, Y.D. Li, Nature **437**, 121 (2005)
7. J.W. Wang, X. Wang, C. Peng, Y.D. Li, Inorg. Chem. **43**, 7552 (2004)
8. K.A. Dick, K. Deppert, M.W. Larsson, T. Martensson, W. Seifert, L.R. Wallenberg, L. Samuelson, Nat. Mater. **3**, 380 (2004)
9. V. Polshettiwar, B. Baruwati, R.S. Varma, ACS Nano **3**, 728 (2009)
10. M.W. Shao, Y.Y. Shan, N.B. Wong, S.T. Lee, Adv. Func. Mater. **15**, 1478 (2005)
11. B. Xue, R. Liu, Z.D. Xu, X.X. Sun, Chinese J. Inorg. Chem. **25**, 1 (2009)
12. W.N. Li, J.K. Yuan, S. Gomez-Mower, S. Sithambaram, S.L. Suib, J. Phys. Chem. B **110**, 3066 (2006)
13. J.C. Yu, A.W. Xu, L.Z. Zhang, R.Q. Song, L. Wu, J. Phys. Chem. B **108**, 64 (2004)
14. Y. Chabre, J. Pannetier, Prog. Solid State Chem. **23**, 1 (1995)
15. L. Espinal, S.L. Suib, J.F. Rusling, J. Am. Chem. Soc. **126**, 7676 (2004)
16. R. Chitrakar, H. Kanoh, Y.S. Kim, Y. Miyai, K. Ooi, J. Solid State Chem. **160**, 69 (2001)
17. A.R. Armstrong, P.G. Bruce, Nature **381**, 499 (1996)
18. D.W. Liu, B.B. Garcia, Q.F. Zhang, Q. Guo, Y.H. Zhang, S. Sepehri, G.Z. Cao, Adv. Funct. Mater. **19**, 1015 (2009)
19. M. Winter, R.J. Brodd, Chem. Rev. **104**, 4245 (2004)
20. M. Toupin, T. Brousse, D. Be'langer, Chem. Mater. **14**, 3946 (2002)
21. A.K.M.F. Ul Islam, R. Islam, K.A. Khan, J. Mater. Sci. Mater. Electr. **16**, 203 (2005)
22. X. Wang, Y.D. Li, Chem. Eur. J. **9**, 300 (2003)
23. D. Portehault, S. Cassaignon, E. Baudrin, J.P. Jolivet, Chem. Mater. **19**, 5410 (2007)
24. Z.Y. Yuan, T.Z. Ren, G.H. Du, B.L. Su, Appl. Phys. A **80**, 743 (2005)
25. L.C. Zhang, Z.H. Liu, H. Lv, X.H. Tang, K. Ooi, J. Phys. Chem. C **111**, 8418 (2007)
26. F.Y. Cheng, J. Chen, X.L. Gou, P.W. Shen, Adv. Mater. **17**, 2753 (2005)
27. D.S. Zheng, S.X. Sun, W.L. Fan, H.Y. Yu, C.H. Fan, G.X. Cao, Z.L. Yin, X.Y. Song, J. Phys. Chem. B **109**, 16439 (2005)
28. F.Y. Cheng, Y. Su, J. Liang, Z.L. Tao, J. Chen, Chem. Mater. **22**, 898 (2010)
29. X.B. Fu, J.Y. Feng, H. Wang, K.M. Ng, Cataly. Commun. **10**, 1844 (2009)
30. L. Jin, C.H. Chen, V.M.B. Crisostomo, L.P. Xu, Y.C. Son, S.L. Suib, Appl. Cataly. A **355**, 169 (2009)
31. S.H. Liang, F.T.G. Bulgan, R.L. Zong, Y.F. Zhu, J. Phys. Chem. C **112**, 5307 (2008)
32. W.X. Zhang, H. Wang, Z.H. Yang, F. Wang, Colloid Surf. A **304**, 60 (2007)
33. X. Wang, Y.D. Li, J. Am. Chem. Soc. **124**, 2880 (2001)
34. R. Sato, Nature **184**, 2005 (1959)
35. M.W. Shao, F. Xu, Y.Y. Peng, J. Wu, Q. Li, S.Y. Zhang, Y.T. Qian, New J. Chem. **26**, 1440 (2002)
36. J. Zeng, C. Liu, J.L. Huang, X.P. Wang, S.Y. Zhang, G.P. Li, J.G. Hou, Nano Lett. **8**, 1318 (2008)
37. D.Y. Zhang, D. Yang, H.J. Zhang, C.H. Lu, L.M. Qi, Chem. Mater. **18**, 3477 (2006)
38. M.W. Shao, L. Cheng, X.H. Zhang, D.D.D. Ma, S.T. Lee, J. Am. Chem. Soc. **131**, 17738 (2009)